



where  $A_{ij}$  is the exchange interaction strength between  $m_i$  and  $m_j$ , which causes adjacent magnetic moments to align parallel to each other. The DMI effect[22] is induced by the bottom heavy metal channel acting on the MTJ free layer, and its equivalent magnetic induction strength is expressed as:

$$\hat{H}_{dmi} = - \sum_{i,j} D_{ij} m_i \times m_j \quad (2)$$

where  $D_{ij}$  is the DMI tensor between  $m_i$  and  $m_j$ , which causes adjacent magnetic moments to align perpendicular to each other.

With the PMA strength held constant, the curling of the free layer magnetization increases gradually with the enhancement of DMI strength. In this study, micromagnetic simulations are performed to investigate the magnetization states of a  $20nm \times 20nm \times 1nm$  free layer under varying perpendicular magnetic anisotropy and DMI strengths at equilibrium. The simulation results are shown in Fig.2.

As shown in Fig.2 (b), when the relative strength of the PMA is significant, the magnetization of the free layer is in region A, exhibiting a uniform state. The vertical stripe structure observed in region B (Fig.2 (c)) characterizes the relative strength of the DMI effect being greater than the PMA at this point. Further curling of the magnetization into circular striped structures (Fig.2 (d)) is observed in region C. In order to ensure that the free-layer magnetic moment can be effectively read through the MTJ, it is necessary to ensure that the MTJ remains uniformly magnetized in the absence of SOT currents (that is the region A in Fig.2 (a)).

Referring to the experimental results of DMI effect[23] and widely used micromagnetic simulation parameters[24], [25], the parameters of the free layer of LVA-MTJ device are as follows: the device size is  $20nm \times 20nm \times 1nm$ , the cell size in *mumax3* is  $1nm \times 1nm \times 1nm$ . The saturation

magnetization strength ( $M_s$ ) is set to  $1.1 \times 10^6 A/m$ , the exchange strength ( $A_{ex}$ ) is  $1.6 \times 10^{-11} J/m$ , the uniaxial perpendicular magnetic anisotropy strength is  $8 \times 10^5 J/m^3$ , the damping factor ( $\alpha$ ) is 0.1, the DMI strength ( $D_{ind}$ ) is  $1 \times 10^{-3} J/m^2$ , the SOT strength coefficient (SOTxi) is  $-2$ , and the polarization strength is 0.15.

The planar schematic of LVA-MTJ, as shown in Fig.3 (a), features four input and output ports. Among these, T1 and T2 serve as the current paths of SOT, influencing the free layer magnetization through the Spin Hall Effect (SHE) effect[26]. The ports T3 and T2 constitute the MTJ structure and are used for the readout of the free layer magnetization. T4 is the VCMA voltage port, which adjusts the local PMA strength by altering the magnitude and polarity of the voltage to influence the flipping of the free layer magnetization.

Before elaborating on the working steps of LVA-MTJ, we need to understand the variation of free layer magnetization of the device under different voltage and current conditions.

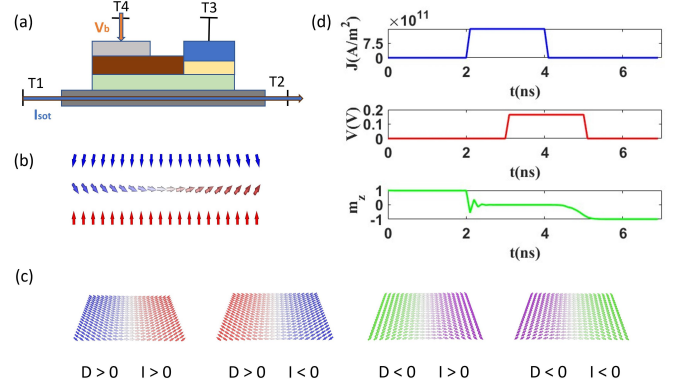


Fig. 3. (a) LVA-MTJ plane schematic diagram. (b) Free layer magnetic moment under SOT current and VCMA voltage. (c) Spin textures under different DMI intensity and current polarity. (d) The magnetic moment of the free layer varies with voltage and current during the writing process.

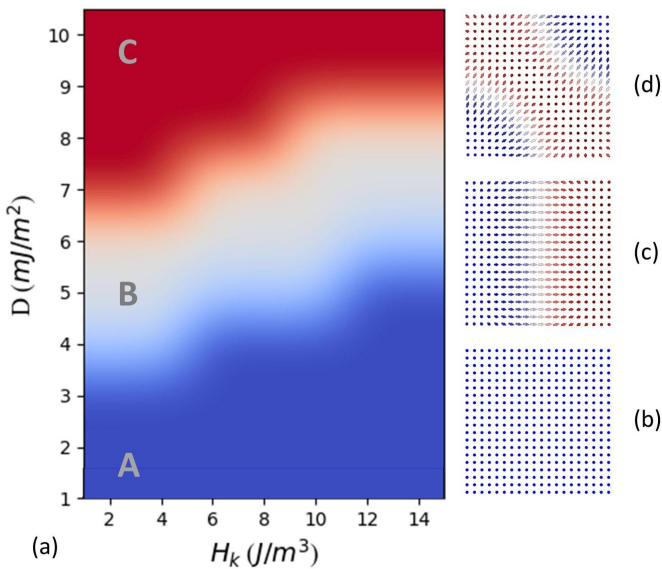


Fig. 2. (a) Diagram of magnetic moment equilibrium state of the free layer under different magnetic parameters, in which the blue, white and red parts correspond to (b) uniform state, (c) vertical fringe structure and (d) circular fringe structure respectively.

As shown in Fig.3 (b), when no SOT current and VCMA voltage are applied, the free layer magnetization aligns uniformly (either up or down spin) under the combined influence of PMA and exchange interaction. When SOT current is applied, the in-plane spin current generated by SHE effect weakens the effect of PMA. Under the influence of DMI effect, the magnetic moment of the free layer presents a chiral spin texture, and the magnetic moment of the free layer is determined by the direction of SOT current and the sign of DMI tensor, as shown in Fig.3 (c). At this time, the application of bias voltage produces a magnetic anisotropy gradient, which makes the free layer magnetic moments in different regions subject to different PMA (The positive bias voltage is used as an example). However, since the DMI effect is dominant, the chiral spin texture does not change. Maintaining the voltage and ceasing the SOT current, the free layer magnetization will return to a uniform state under the influence of exchange interaction. In this scenario, regions with stronger anisotropy exhibit greater flipping force, thus the final magnetization of the free layer will uniformly align towards the direction of stronger anisotropy. Therefore, deterministic reversal of

the free layer magnetic moment can be achieved without an external magnetic field, enabling information writing.

From Fig.3 (d), it can be observed that the write process of LVA-MTJ consists of three main steps. The first step involves applying a SOT charge current of  $150\text{MA}/\text{cm}^2$  to the free layer from the T1 and T2 ports to induce the formation of a chiral spin texture. In the second step, the SOT current is maintained and a voltage of  $\pm 0.165\text{V}$  is applied to terminal T4 to modify the magnetic anisotropy. The functional relationship between the voltage and the anisotropy is determined as follows[27], [28]:

$$H_k(V_b) = H_k(0) - \beta V_b/t_{ox} \quad (3)$$

where  $\beta$  is the VCMA coefficient, here is  $9.0429 \times 10^{-5} \text{J}/\text{V}$ , and  $t_{ox}$  is the thickness of the insulator layer. In the third step, the SOT current is removed while keeping the voltage at the T4 terminal unchanged. Under the influence of the differences in magnetic anisotropy, the magnetization undergoes directed flipping, completing the information writing process. The resistance state of the MTJ can be read directly by applying current to the T3 and T2 terminals.

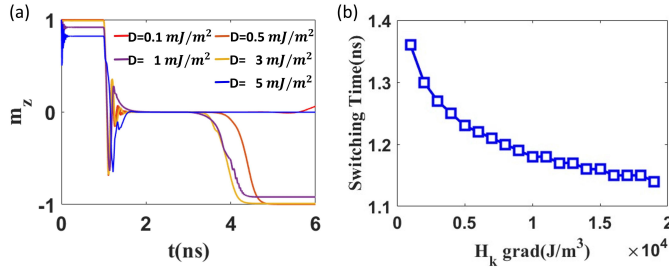


Fig. 4. (a)The process of information inscribing varies with DMI strength.(b)The change of the time for the free layer to return to the uniform state with the anisotropy gradient after the release of SOT current.

The magnitude of the anisotropy gradient and variations in DMI strength have an impact on the information writing process of the device. On the one hand, as shown in Fig.4 (a), the effect of DMI strength on the information writing process is complex. When the DMI strength is too weak, an effective chiral spin texture cannot be formed to support the directed flipping of the free layer. After applying the SOT current, the free layer magnetization remains in an intermediate state for a relatively long time. Conversely, when the DMI strength is too strong, even the chiral spin texture formed by removing the SOT current is difficult to break by the perpendicular magnetic anisotropy field, ultimately remaining in the intermediate state. In the intermediate state between the two extremes, an increase in the DMI effect leads to a gradual strengthening of magnetization fluctuation during the formation of the chiral spin texture under the influence of the SOT current. Furthermore, the recovery time after removing the SOT current also gradually lengthens. This reflects the weakening effect of DMI on the uniform magnetic state.

On the other hand, the variation in the magnitude of magnetic anisotropy gradient has little effect on the formation of self-selected textures when subject to SOT current. However, it slightly alters the time required for the free layer magnetization

to recover from a chiral spin texture to a uniform magnetic state during the release of the SOT current, as depicted in Fig.4 (b). More specifically, the increase in the average magnetic anisotropy gradient (decrease in the average value of the anisotropy field) leads to a reduction in the time required to return to a uniform magnetic state.

### III. CONCLUSION

In this work, a field-free MTJ device based on the localized VCMA effect and DMI effect-mediated SOT switch is proposed. By locally applying the VCMA effect to the free layer to construct a PMA gradient, and ultimately combining it with the non-collinear spin texture formed by the DMI effect under the SOT current, deterministic switching of the free layer magnetization in the MTJ can be achieved without an external magnetic field. Through micromagnetic simulations, we effectively analyze the stable states and operating modes of the LVA-MTJ free layer. In addition, the scalability of DMI intensity and PMA gradient is also discussed. This work provides a feasible solution for the design of future field-free spintronic devices.

### REFERENCES

- [1] S. M. Alam, S. Ikegawa, K. Nagel, F. Mancoff, M. DeHerrera, F. Neumeyer, J. T. Williams, I. Rahman, A. Shah, Y. Kim, and S. Aggarwal, "Versatile STT-MRAM architecture for memory and emerging applications," in *2023 IEEE 34th Magnetic Recording Conference (TMR)*, Minneapolis, MN, USA, July 2023, pp. 1–2.
- [2] T. Na, S. H. Kang, and S.-O. Jung, "STT-MRAM sensing: A review," *IEEE Trans. Circuits Syst. II*, vol. 68, no. 1, pp. 12–18, Jan. 2021.
- [3] T. Nozaki, T. Yamamoto, S. Miwa, M. Tsujikawa, M. Shirai, S. Yuasa, and Y. Suzuki, "Recent progress in the voltage-controlled magnetic anisotropy effect and the challenges faced in developing voltage-torque MRAM," *Micromachines*, vol. 10, no. 5, p. 327, May 2019.
- [4] K. Garello, F. Yasin, H. Hody, S. Couet, L. Souriau, S. H. Sharifi, J. Swerts, R. Carpenter, S. Rao, W. Kim, J. Wu, K. K. V. Sethu, M. Pak, N. Jossart, D. Crotti, A. Furnémont, and G. S. Kar, "Manufacturable 300nm platform solution for field-free switching sot-mram," *2019 Symposium on VLSI Circuits*, pp. T194–T195, 2019.
- [5] V. K. Joshi, P. Barla, S. Bhat, and B. K. Kaushik, "From MTJ device to hybrid CMOS/MTJ circuits: A review," *IEEE Access*, vol. 8, pp. 194 105–194 146, 2020.
- [6] S.-h. C. Baek, V. P. Amin, Y.-W. Oh, G. Go, S.-J. Lee, G.-H. Lee, K.-J. Kim, M. D. Stiles, B.-G. Park, and K.-J. Lee, "Spin currents and spin-orbit torques in ferromagnetic trilayers," *Nature Mater*, vol. 17, no. 6, pp. 509–513, June 2018.
- [7] C. Wang, Z. Wang, M. Wang, X. Zhang, Y. Zhang, and W. Zhao, "Compact model of dzyaloshinskii domain wall motion-based MTJ for spin neural networks," *IEEE Trans. Electron Devices*, vol. 67, no. 6, pp. 2621–2626, June 2020.
- [8] N. Zogbi, S. Liu, C. H. Bennett, S. Agarwal, M. J. Marinella, and J. A. C. Incorvia, "Parallel matrix multiplication using voltage-controlled magnetic anisotropy domain wall logic," *IEEE Journal on Exploratory Solid-State Computational Devices and Circuits*, vol. 9, no. 1, 2023.
- [9] S. Luo, M. Song, M. Shen, Y. Zhang, J. Hong, and L. You, "Skyrmion latch and flip-flop in magnetic nanotracks with gradient anisotropy," *Journal of Magnetism and Magnetic Materials*, vol. 494, p. 165739, Jan. 2020.
- [10] Y. Tokura and N. Kanazawa, "Magnetic skyrmion materials," *Chem. Rev.*, vol. 121, no. 5, pp. 2857–2897, Mar. 2021.
- [11] W. Kang, C. Zheng, Y. Huang, X. Zhang, Y. Zhou, W. Lv, and W. Zhao, "Complementary skyrmion racetrack memory with voltage manipulation," *IEEE Electron Device Lett.*, vol. 37, no. 7, pp. 924–927, July 2016.
- [12] S. Z. Peng, J. Q. Lu, W. X. Li, L. Z. Wang, H. Zhang, X. Li, K. L. Wang, and W. S. Zhao, "Field-free switching of perpendicular magnetization through voltage-gated spin-orbit torque," in *2019 IEEE International Electron Devices Meeting (IEDM)*, San Francisco, CA, USA, Dec. 2019, pp. 28.6.1–28.6.4.

- [13] S. Alla, V. Kumar Joshi, and S. Bhat, "Field-free switching of VG-SOT-pMTJ device through the interplay of SOT, exchange bias, and VCMA effects," *Journal of Applied Physics*, vol. 134, no. 1, p. 013901, July 2023.
- [14] T. Moriya, "Anisotropic superexchange interaction and weak ferromagnetism," *Phys. Rev.*, vol. 120, no. 1, pp. 91–98, Oct. 1960.
- [15] G. Yu, P. Upadhyaya, Y. Fan, J. G. Alzate, W. Jiang, K. L. Wong, S. Takei, S. A. Bender, L.-T. Chang, Y. Jiang, M. Lang, J. Tang, Y. Wang, Y. Tserkovnyak, P. K. Amiri, and K. L. Wang, "Switching of perpendicular magnetization by spin-orbit torques in the absence of external magnetic fields," *Nature Nanotech.*, vol. 9, no. 7, pp. 548–554, July 2014.
- [16] H. Wu, J. Nance, S. A. Razavi, D. Lujan, B. Dai, Y. Liu, H. He, B. Cui, D. Wu, K. Wong, K. Sobotkiewich, X. Li, G. P. Carman, and K. L. Wang, "Chiral symmetry breaking for deterministic switching of perpendicular magnetization by spin-orbit torque," *Nano Lett.*, vol. 21, no. 1, pp. 515–521, Jan. 2021.
- [17] P. Khalili Amiri, J. G. Alzate, X. Q. Cai, F. Ebrahimi, Q. Hu, K. Wong, C. Grezes, H. Lee, G. Yu, X. Li, M. Akyol, Q. Shao, J. A. Katine, J. Langer, B. Ocker, and K. L. Wang, "Electric-field-controlled magnetoelectric RAM: Progress, challenges, and scaling," *IEEE Trans. Magn.*, vol. 51, no. 11, pp. 1–7, Nov. 2015.
- [18] W. Kang, Y. Huang, C. Zheng, W. Lv, N. Lei, Y. Zhang, X. Zhang, Y. Zhou, and W. Zhao, "Voltage controlled magnetic skyrmion motion for racetrack memory," *Sci Rep*, vol. 6, no. 1, p. 23164, Mar. 2016.
- [19] A. H. Lone and H. Fariborzi, "Skyrmion-magnetic tunnel junction synapse with long-term and short-term plasticity for neuromorphic computing," *IEEE Trans. Electron Devices*, vol. 70, no. 1, pp. 371–378, Jan. 2023.
- [20] A. Vansteenkiste, J. Leliaert, M. Dvornik, M. Helsen, F. Garcia-Sanchez, and B. Van Waeyenberge, "The design and verification of MuMax3," *AIP Advances*, vol. 4, no. 10, p. 107133, Oct. 2014.
- [21] A. Aharoni, *Introduction to the Theory of Ferromagnetism*. Clarendon Press, 2000, vol. 50, cit. on pp. 11, 19, 31.
- [22] I. Dzyaloshinsky, "A thermodynamic theory of "weak" ferromagnetism of antiferromagnetics," *Journal of Physics and Chemistry of Solids*, vol. 4, no. 4, pp. 241–255, Jan. 1958.
- [23] S. Yuasa, A. Fukushima, K. Yakushiji, T. Nozaki, M. Konoto, H. Maehara, H. Kubota, T. Taniguchi, H. Arai, H. Imamura, K. Ando, Y. Shiota, F. Bonell, Y. Suzuki, N. Shimomura, E. Kitagawa, J. Ito, S. Fujita, K. Abe, K. Nomura, H. Noguchi, and H. Yoda, "Future prospects of MRAM technologies," in *2013 IEEE International Electron Devices Meeting*, Washington, DC, USA, Dec. 2013, pp. 3.1.1–3.1.4.
- [24] F. Büttner, I. Lemesch, M. Schneider, B. Pfau, C. M. Günther, P. Hessing, J. Geilhufe, L. Caretta, D. Engel, B. Krüger, J. Viefhaus, S. Eisebitt, and G. S. D. Beach, "Field-free deterministic ultra fast creation of skyrmions by spin orbit torques," *Nature Nanotech.*, vol. 12, no. 11, pp. 1040–1044, Nov. 2017.
- [25] J. Leliaert, B. Van de Wiele, A. Vansteenkiste, L. Laurson, G. Durin, L. Dupré, and B. Van Waeyenberge, "Creep turns linear in narrow ferromagnetic nanostrips," *Sci Rep*, vol. 6, no. 1, p. 20472, Feb. 2016.
- [26] J. Sinova, S. O. Valenzuela, J. Wunderlich, C. H. Back, and T. Jungwirth, "Spin hall effect," Nov. 2014.
- [27] H. Lee, A. Lee, F. Ebrahimi, P. Khalili Amiri, and K. L. Wang, "Analog to stochastic bit stream converter utilizing voltage-assisted spin hall effect," *IEEE Electron Device Lett.*, vol. 38, no. 9, pp. 1343–1346, Sept. 2017.
- [28] W. Kang, Y. Ran, Y. Zhang, W. Lv, and W. ZHAO, "Modeling and exploration of the voltage controlled magnetic anisotropy effect for the next-generation low-power and high-speed MRAM applications," *IEEE Transactions on Nanotechnology*, vol. PP, pp. 1–1, Jan. 2017.